Guanine quadruplex structures localize to heterochromatin

Hoffmann, Roland F.; Moshkin, Yuri M.; Mouton, Stijn; Grzeschik, Nicola A.; Kalicharan, Ruby D.; Kuipers, Jeroen; Wolters, Anouk H. G.; Nishida, Kazuki; Romashchenko, Aleksander V.; Postberg, Jan

Published in:
Nucleic Acids Research

DOI:
10.1093/nar/gkv900

Publication date:
2016

152–163 *Nucleic Acids Research, 2016, Vol. 44, No. 1* *Published online 17 September 2015*
doi: 10.1093/nar/gkv900

Guanine quadruplex structures localize to heterochromatin

Roland F. Hoffmann[1], Yuri M. Moshkin[2], Stijn Mouton[1], Nicola A. Grzeschik[3], Ruby D. Kalicharan[3], Jeroen Kuipers[3], Anouk H.G. Wolters[3], Kazuki Nishida[4], Aleksander V. Romashchenko[2,5], Jan Postberg[6], Hans Lipps[7], Eugene Berezikov[1,5], Ody C.M. Sibon[3], Ben N.G. Giepmans[3] and Peter M. Lansdorp[1,8,*]

[1]European Research Institute for the Biology of Ageing, University of Groningen, University Medical Centre Groningen, A. Deusinglaan 1, NL-9713 AV Groningen, The Netherlands, [2]Department of Biochemistry, Erasmus University Medical Center, Dr. Molewaterplein 50, NL-3015 GE Rotterdam, The Netherlands, [3]Department of Cell Biology, University of Groningen, University Medical Centre Groningen, A. Deusinglaan 1, NL-9713 AV Groningen, The Netherlands, [4]Faculty of Medicine, Kyoto University, Kyoto 606-8501, Japan, [5]Institute of Cytology and Genetics, Siberian Branch of the Russian Academy of Sciences, Novosibirsk 630090, Russia, [6]Helios Medical Centre Wuppertal, Paediatrics Centre, Witten/Herdecke University, Wuppertal, Germany, [7]Institute of Cell Biology, Centre for Biomedical Education and Research, Witten/Herdecke University, Witten, Germany and [8]Terry Fox Laboratory, British Columbia Cancer Agency and Department of Medicine, University of British Columbia Vancouver, BC, V5Z 1L3, Canada

Received June 26, 2015; Revised August 19, 2015; Accepted August 21, 2015

ABSTRACT

Increasing amounts of data support a role for guanine quadruplex (G4) DNA and RNA structures in various cellular processes. We stained different organisms with monoclonal antibody 1H6 specific for G4 DNA. Strikingly, immuno-electron microscopy showed exquisite specificity for heterochromatin. Polytene chromosomes from *Drosophila* salivary glands showed bands that co-localized with heterochromatin proteins HP1 and the SNF2 domain-containing protein SUUR. Staining was retained in SUUR knock-out mutants but lost upon overexpression of SUUR. Somatic cells in *Macrostomum lignano* were strongly labeled, but pluripotent stem cells labeled weakly. Similarly, germline stem cells in *Drosophila* ovaries were weakly labeled compared to most other cells. The unexpected presence of G4 structures in heterochromatin and the difference in G4 staining between somatic cells and stem cells with germline DNA in ciliates, flatworms, flies and mammals point to a conserved role for G4 structures in nuclear organization and cellular differentiation.

INTRODUCTION

The mechanisms and processes that govern the organization of DNA in eukaryotic chromosomes and cells are incompletely understood (1). In nuclei dense areas of heterochromatin can typically be distinguished next to more open areas of euchromatin (2,3). How these different morphologies relate to known chromatin features such as histone modifications, DNA methylation and non-coding RNA is subject of intense research efforts (4,5). Similarly, the organization of chromatin in mitotic chromosomes remains unclear. Recent data challenge the classic model in which 10-nm DNA fibers are folded into 30-nm chromatin fibers (6,7). Instead, it was proposed that packaging of 10-nm DNA fibers is achieved in a 'fractal manner' whereby DNA fibers fold back and interact at many different levels (8).

In vitro, single stranded guanine-rich RNA or DNA readily adopts higher order structures known as guanine quadruplex (G4) structures (9). Extensive studies have documented that the formation and stability of G4 structures under physiological conditions depends on many factors including the concentrations of various ions in the nucleus (10,11). G4 formation could furthermore depend on the presence of specific proteins and their post-translational modifications, non-coding RNA's and factors that influence the stability of duplex DNA such as cytosine methylation (12) and DNA supercoiling (13). Sequences capable of forming G4 DNA are abundant in human DNA (14–16) and such sequences are enriched in promoters and the first intron of many genes and at telomeres (17). Whereas G4 RNA could presumably readily form in specific G-rich transcripts, it is typically assumed that guanine-rich DNA must dissociate from its complementary C-rich sequences

*To whom correspondence should be addressed. Tel: +31 50 361 7300; Fax: +31 50 361 7300; Email: p.m.lansdorp@umcg.nl

and be single stranded in order for G4 DNA to form. In principle, this could occur during transcription (18), replication (19–21) or DNA repair. In addition, G4 DNA could form at telomeres either at the 3' single strand G-rich overhang (22) or by molecular crowding of duplex DNA (23). Recently, it was proposed that the transition of duplex DNA to quadruplex DNA could serve as a reversible cellular signal promoted by negative supercoiling of DNA (13). Despite accumulating evidence supporting a role for G4 RNA and DNA in diverse biological processes (24,25), detection of G4 structures *in situ* has been problematic in part because suitable reagents to detect G4 structures have been lacking.

We recently described a mouse monoclonal antibody, 1H6, which strongly binds ($K_d = 0.3$nM) to synthetic interas well as intramolecular G4 DNA structures (26). The specificity of 1H6 for various G4 DNA structures was validated *in vitro* and *in vivo* and epitopes recognized by 1H6 in cells were found to be sensitive to DNAse treatment but resistant to RNAse. Staining intensity increased following incubation with G4 stabilizing ligands and all human tissues tested showed strong nuclear staining as assessed by light microscopy with notable exception of some cells in the testis.

In our current study we extended our observations with the 1H6 antibody to include different species and we performed 1H6 immuno-electron microscopy (EM). Surprisingly, we found that staining is very specific for heterochromatin in all species tested and heterochromatic regions of *Drosophila* salivary gland polytene chromosomes. Furthermore, we found that staining is not only very weak in some cells of human testis but also in cells with germline DNA from ciliates, flatworms and flies.

MATERIALS AND METHODS

General

Fluorescent secondary antibodies, kits or dyes were from Molecular Probes, Invitrogen (Grand Island, NY), unless stated otherwise. Specimens were analyzed with a Zeiss-LSM780 NLO confocal microscope. All EM samples were analyzed with either an FEI Cm100 or a Zeiss Supra 55 STEM microscope. ATLAS large scale scan generator (Fibics, Canada) was used for large scale imaging (nanotomy). Data sampling is explained online (www.nanotomy.org). Data analysis was performed with the Fibics VEviewer, Zeiss Zen software, Huygens Deconvolution software, Imaris, ImageJ and Adobe Photoshop. Image assembly was done using Adobe Illustrator and Microsoft Powerpoint. Abbreviations: PBS = Phosphate Buffered Saline; TBS = Tris Buffered Saline; BSA = Bovine Serum Albumin; NGS = Normal Goat Serum, RT = Room Temperature.

Animals and cells

Rats - Analysis of Islets of Langerhans cells from rat pancreas was performed on embedded tissue as described before (27). *Macrostomum lignano* was maintained under standard conditions at 20°C degrees. *Drosophila melanogaster w1118* control flies were raised on standard cornmeal agar food at 25°C. Salivary glands for polytene chromosome stainings were dissected from third instar larvae, ovaries were collected and dissected from 3–4 day old adult females. *PANC-1 (human pancreatic carcinoma)* cells were cultured under standard conditions. Cells were plated on glass-bottom dishes to analyze mitotic cells.

Immuno electron microscopy

Drosophila ovaries and rat pancreatic tissue were fixed overnight at 4°C in 2% glutaraldehyde buffered in 0.1M cacodylate and PANC-1 cells were fixed for 1 h. For *Macrostomum lignano* 10% sucrose was added to the fixative. After fixation all samples were washed in 0.1M cacodylate buffer and post-fixed in 1% OsO_4 / 1.5% $K_3Fe(CN_6)$ for 30–60 min, dehydrated and embedded in epoxy resin according to standard protocols. 60 nm sections were collected on nickel grids, treated with 1% periodic acid for 20 min at RT, rinsed with distilled water (3 × 5 min, RT) and blocked in blocking buffer (TBS containing 1% BSA, 0.1% Glycine, 0.1% cold water fish skin gelatin and 5% normal goat serum). The grids were incubated overnight with monoclonal mouse 1H6 (0.5–1 μg/ml) in blocking buffer with 1% normal goat serum) at 4°C, rinsed in TBS (3 × 5 min, RT), followed by incubation with secondary antibody, conjugated to 10 nm gold (British Biocell International; 1:50 in blocking buffer) for 2 h at RT. Samples were rinsed 3x 5' with distilled water and contrasted with uranyl acetate and lead citrate. 1H6 was produced in house and is available from MediMabs (Montreal).

Stylonychia immunofluorescence

For G-quadruplex DNA staining using 1H6 *Stylonychia* cells were collected on a 30 μm gauze, washed with PBS and resuspended in 1 ml ice-cold nuclei lysis buffer (0.8% IGEPAL CA-630, 0.3 M sucrose, 15 mM NaCl, 5mM $MgCl_2$, 0.1 mM EGTA, 15 mM Tris–HCl pH 7.5, 0.5 mM DTT, 0.1 mM PMSF, 3.6 ng/ml aprotinin). The suspension was then layered onto a sucrose cushion (1.6 M sucrose, 15 mM NaCl, 5mM $MgCl_2$, 0.1 mM EGTA, 15 mM Tris–HCl pH 7.5, 0.5 mM DTT, 0.1 mM PMSF, 3.6 ng/ml aprotinin) and centrifuged at 4000 rpm using a Heraeus Megafuge for 45 min at 4°C. The supernatant was carefully removed before nuclei were fixed in PBS with 1% formaldehyde for 10 min at room temperature. They were then washed with PBS, and subsequently incubated with glycine stop solution, followed by additional washing with PBS. Nuclei were then incubated 1 h at RT in blocking buffer (PBS with 0.1% BSA and 0.05% Tween 20). 1H6 mouse monoclonal antibody binding was subsequently allowed for 1 h at RT (1 μg/ml 1H6 in PBS, 0.1%BSA, 0.05% Tween 20, 1% DMSO). For secondary detection, after washing the nuclei 2x in PBS, rabbit anti-mouse Alexa-Fluor 433 pAbs (Molecular Probes) were diluted 1:200 in PBS, 0.1%BSA, 0.05% Tween 20, 1% DMSO and incubated 1 h at RT. For counterstaining propidium iodide was used upon manufacturers' suggestion (Molecular Probes). After several washes using PBS nuclei were mounted using adhesive slides and Vectashield mounting medium. Immunofluorescence confocal laser scanning microscopy was performed using the protocol, antibodies and dyes described in detail previously

(28). Images were assembled using ImageJ (Rasband, W.S., National Institutes of Health, Bethesda, Maryland, USA; http://rsb.info.nih.gov/ij/) and Adobe Photoshop CS5 software.

Macrostomum lignano immunohistochemistry

Mature worms were pulsed for 30 min with EdU, relaxed in 1:1 (v/v) $MgCl_2.6H_2O$ (7.14%) - f/2 and fixed in 4% paraformaldehyde containing 0,1% Trition X-100 for 30 min. Subsequently, worms were washed with f/2 (5x) and permeabilized for 1 h with PBS containing 0.25% NP-40 followed by blocking overnight in PBS containing 0.25% NP-40, 300mM glycine and 5% (w/v) BSA (blocking medium). S-phase cells were detected using the Click-It Alexa-Fluor-488 Imaging Kit, according to the manufacturer's specifications. After washing in PBS containing 0.25% NP-40 (3x) and blocking medium (2x) the worms were incubated with mouse monoclonal antibody 1H6 at 2.0 μg/ml in blocking medium followed by rabbit anti-phospho-Histone H3 antibody (Millipore, 1:250) for mitotic cell staining, for 2–4 h at RT in blocking medium (shaking gradually) and kept overnight at 4°C. Worms were washed with PBS containing 0.25% NP-40 (3x) and blocking medium (2x) followed by incubation with secondary antibodies (1:1000), conjugated to Alexa-Fluor-405 and Alexa-Fluor-546 for 4 h at RT in blocking medium (while shaking). After washing with PBS containing 0.25% NP-40 (2x) and PBS (3x), the worms were counterstained with NucRed™ Dead 647 and mounted in Prolong Gold anti-fade reagent (Molecular probes).

To calculate 1H6 fluorescence of $EdU^-/H3^-$, $Edu^+/H3^-$ and $EdU^-/H3^+$ cells in whole mount preparation of labeled worms we used ImageJ software (v 1.49, NIH). An outline was drawn around a cell of interest and the mean gray value and integrated density were measured for each fluorescence channel. In addition, several background readings outside the cell area were performed. Corrected total cell fluorescence (CTCF) for each fluorescence channel was calculated as described (29). Finally, the ratio CTCF (1H6) / CTCF (DAPI) was determined.

Drosophila melanogaster immunohistochemistry

Drosophila ovaries were collected in cold PBS and fixed in 4% formaldehyde (from methanol-free 16% Formaldehyde Solution, Thermo Scientific) for 30–45 min at RT. Fixed tissue was washed in PBS-T (PBS containing 0.1% Triton-X-100) for 1 h at RT. To make the DNA more accessible for the 1H6 antibody and reduce unspecific background, the ovaries were permeabilized and blocked for 30 min in PBS-T containing 5%BSA before incubation with the primary antibodies. The primary antibodies were mouse 1H6 (1.0 μg/ml) and rabbit anti-Vasa (a kind gift from P. Lasko, McGill, Montreal, Canada) used at a 1:500 dilution, overnight at 4°C. After a wash in PBS-T for 1 h at RT the samples were incubated in secondary antibodies and dyes for 2 h at RT. The secondary antibodies, conjugated to Alexa-Fluor-488 or Alexa-Fluor-594, were used at 1:500 dilutions. F-actin was detected with Rhodamin-Phalloidin (20U/ml) and DNA by staining with DAPI (0.2 μg/ml). After one final wash in PBS-T for 1 h at RT the samples were mounted in 80% glycerol and analyzed.

Salivary glands for polytene chromosome stainings were dissected in PBS from third instar larvae followed by fixation for 5 min with 45% acetic acid - 3.7% formaldehyde. Chromosomes were spread by squashing on slides. Slides were frozen in liquid nitrogen and the coverslips were snapped off. Slides were blocked in PBS-1% Triton X-100 (PBST) containing 5% BSA for 30 min at room temperature and incubated overnight with primary antibodies in PBST-1% BSA at 4°C. The primary antibodies were mouse 1H6 (5 μg/ml), rabbit anti-HP1 (1:400, a gift from C.P. Verrijzer), rabbit anti-polII (1:200, a gift from C.P. Verrijzer) and guinea pig anti-SUUR (1:200, a gift from C.P. Verrijzer). The slides then were washed three times for 15 min each time in PBST, and incubated with the appropriate fluorescent secondary antibodies in PBST-1% BSA for 1h at room temperature. The slides then were washed three times in PBST, air dried and mounted in mounting medium with 4′,6′-diamidino-2-phenylindole (DAPI) counterstain (Vectashield with DAPI; H-1200; Vector Laboratories).

RESULTS

G4 structures in the ciliate *Stylonychia*

DNA in the macronucleus of *Stylonychia* is organized in short 'nanochromosomes' ranging in size between about 500bp up to 40kbp with an average size of about 2.7 kb. The telomere of each of these nanochromosomes consists of a 20mer of double stranded 5' $C_4A_4C_4A_4$ and a 3'-single stranded overhang of 16 nucleotides with the sequence $G_4T_4G_4T_4$ (30). With around 16.000 different nanochromosomes, each of which has ≈15.000 copies, a single macronucleus contains an estimated 5×10^8 telomeres (31). The first direct evidence that ciliate telomeres adopt an antiparallel intermolecular G4 structure came from studies using single chain antibodies directed against the parallel or antiparallel ciliate telomeric G4 structure (32). Telomeric sequences in *Stylonychia* appear to be organized in foci bound to a subnuclear structure (33,34) as was suggested by earlier electron microscopy (EM) studies (35,36) and most likely adopt an antiparallel G4 structure (37). Replication of individual nanochromosomes starts at or close to the telomeres (38) and in the macronucleus it takes place within hundreds of synchronously firing replication foci, forming a migrating morphological distinct region, the replication band (39). Importantly, the replication band could not be stained with the phage display antibody in support of the notion that G4 structures are resolved during DNA replication (32).

1H6 staining of replicating macronuclei with 1H6 revealed a staining pattern similar to that previously observed (32). Foci-like structures were observed in macronuclei during interphase and S-phase, but neither in replication bands during S-phase, nor in micronuclei with germline DNA (Figure 1, arrows and asterisks in bottom panels). Of note, the DNA in replication bands was clearly stained by the dye DAPI. Telomeres cluster at the nuclear matrix in the macronucleus via tightly bound proteins such as TEBPα and TEBPβ (40). Whereas such proteins could limit accessibility of the antibody to potential binding sites, such limitations are not expected during DNA replication when telom-

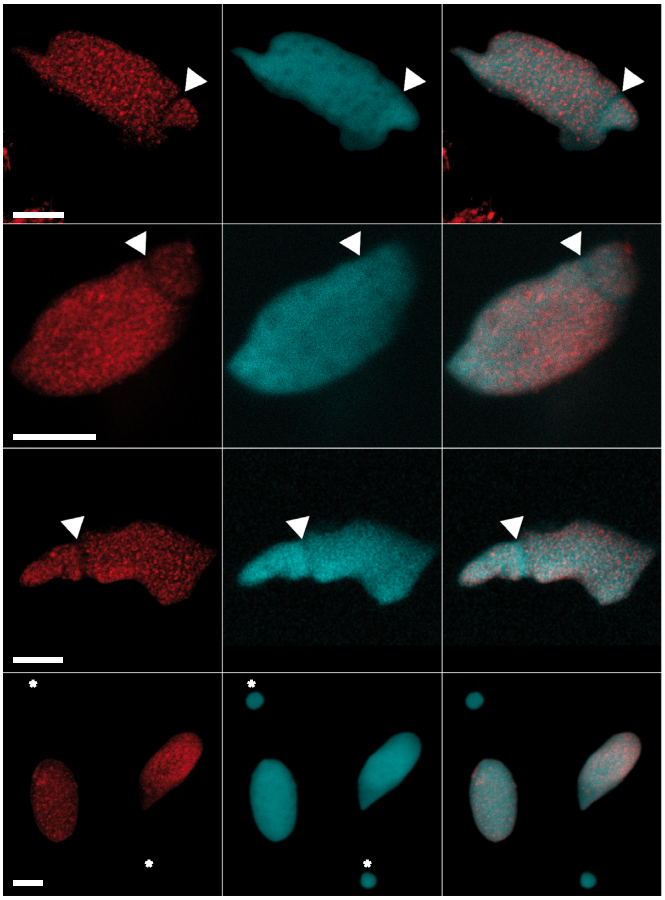

Figure 1. Staining of G4 DNA in the macronucleus of *Stylonychia lemnea*. Indirect immunofluorescence of *Stylonychia* using monoclonal antibody 1H6. Shown are different adult animals with a characteristic staining pattern that excludes the replication band (arrows) as well as the micronucleus (bottom panels, asterisks). The left panels show 1H6 staining, the second row corresponding DAPI staining and the third column an overlay of 1H6 and DAPI fluorescence. Scale bars: 10 μm.

eres dissociate from the nuclear matrix following phosphorylation of TEBPβ (41,42).

G4 structures in the regenerative flatworm *Macrostomum lignano*

Unlike all other cells in human tissues, some cells in human testis were previously found to be unlabeled or only weakly labeled by 1H6 (26). Such poorly labeled cells were found at similar positions to cells expressing high levels of **R**egulator of **Te**lomere **L**ength 1 (RTEL1) (43), a helicase implicated in the processing of G4 DNA (43,44). RTEL1 is essential for proliferative expansion and differentiation of stem cells in flatworms (45) and we considered the possibility that resolution or suppression of G4 structures is important for stem cells with regenerative potential. To test this hypothesis we studied binding of 1H6 to primitive stem cells in two model organisms: the flatworm *Macrostomum lignano* (46) (Figure 2) and *Drosophila melanogaster* (47) (Figure 3). Pluripotent stem cells in *Macrostomum,* called neoblasts, can give rise to somatic cells as well as cells of the germline (48) and stem cells of the germline are located at well-defined positions in the ovaries of *Drosophila* (49,50). Immuno-EM of *Macrostomum lignano* showed that 1H6 antibody binds primarily to nuclear heterochromatin (Figure 2). This is illustrated for an epidermal cell and a neoblast (51) in respectively Figure 2C and D. Specific cell types in *Macrostomum lignano* were also identified following 1H6 staining using confocal microscopy. Neoblasts and germline cells, the only proliferating cells in adult animals (52), were identified by incorporation of the nucleoside analog EdU to label S-phase cells and by staining for phospho-histone H3 to identify mitotic cells. While most nuclei in adult *Macrostomum* were brightly labeled by 1H6, staining of neoblasts and proliferating cells in the germline was much weaker (Figure 2E-F and Supplementary Figure S1 and Movies 1 and 2). Fluorescence measurements of individual nuclei confirmed a significant difference in 1H6 fluorescence between proliferating and quiescent cells (ratio of integrated 1H6 fluorescence intensity relative to DAPI fluorescence intensity ± standard deviation for somatic, $EdU^-/H3^-$ cells = 1.04 ± 0.12; S-phase $EdU^+/H3^-$ cells = 0.65 ± 0.05 and M-phase $EdU^-/H3^+$ cells = 0.58 ± 0.10; $n = 5$; $P < 0.05$). Not all neoblast have the same developmental potential (53) and some of the differences in 1H6 staining between $EdU^+/H3^-$ cells could reflect neoblast lineage commitment or differentiation. We conclude that neoblasts and cells of the germline in *Macrostomum* show less 1H6 staining and that heterochromatin staining and 1H6 staining appear to be correlated in this species.

1H6 staining of *Drosophila melanogaster*

We next studied G4 DNA in stem cells of the germline in ovaries of *Drosophila melanogaster*. Each ovariole, the basic structural unit of the ovary, consists of a germarium and a string of maturing egg chambers (Figure 3A,B). At the tip of each germarium (Figure 3B), two to three germline stem cells (GSCs) and a number of somatic cells can be identified. GSCs undergo asymmetric cell divisions to give rise to another stem cell as well as a cystoblast (CB) which, upon further division, produces 2-cell, 4-cell, 8-cell and 16-cell germline cysts (50). Mature cysts, comprised of 15 nurse cells (NC) and a presumptive oocyte (O), are covered by follicle cells (FCs) (Figure 3B). GSCs and mature nurse cells showed only weak staining by 1H6 (Figure 3F and G). In contrast, the oocyte nucleus and most somatic cell nuclei were brightly labeled (Figure 3F, Supplementary Figure S2). Reduced 1H6 staining of GSCs was confirmed by EM, which also showed less heterochromatin per nuclear surface area in GSCs compared to other cells located in the germarium (Figure 3C-E, boxed inserts and corresponding nanotomy scale images).

Staining of *Drosophila* polytene chromosomes

To further study the link between heterochromatin and G4 DNA we performed 1H6 staining of polytene chromosomes from *Drosophila* third instar stage salivary glands. Such chromosomes contain heterochromatic bands that are typically underreplicated during endoreplication cycles (54–56). 1H6 showed bright staining of pericentric heterochromatin, ANTP-C and BX-C (57) and a large number of additional bands (Figure 4, middle panels). Antibodies to HP1

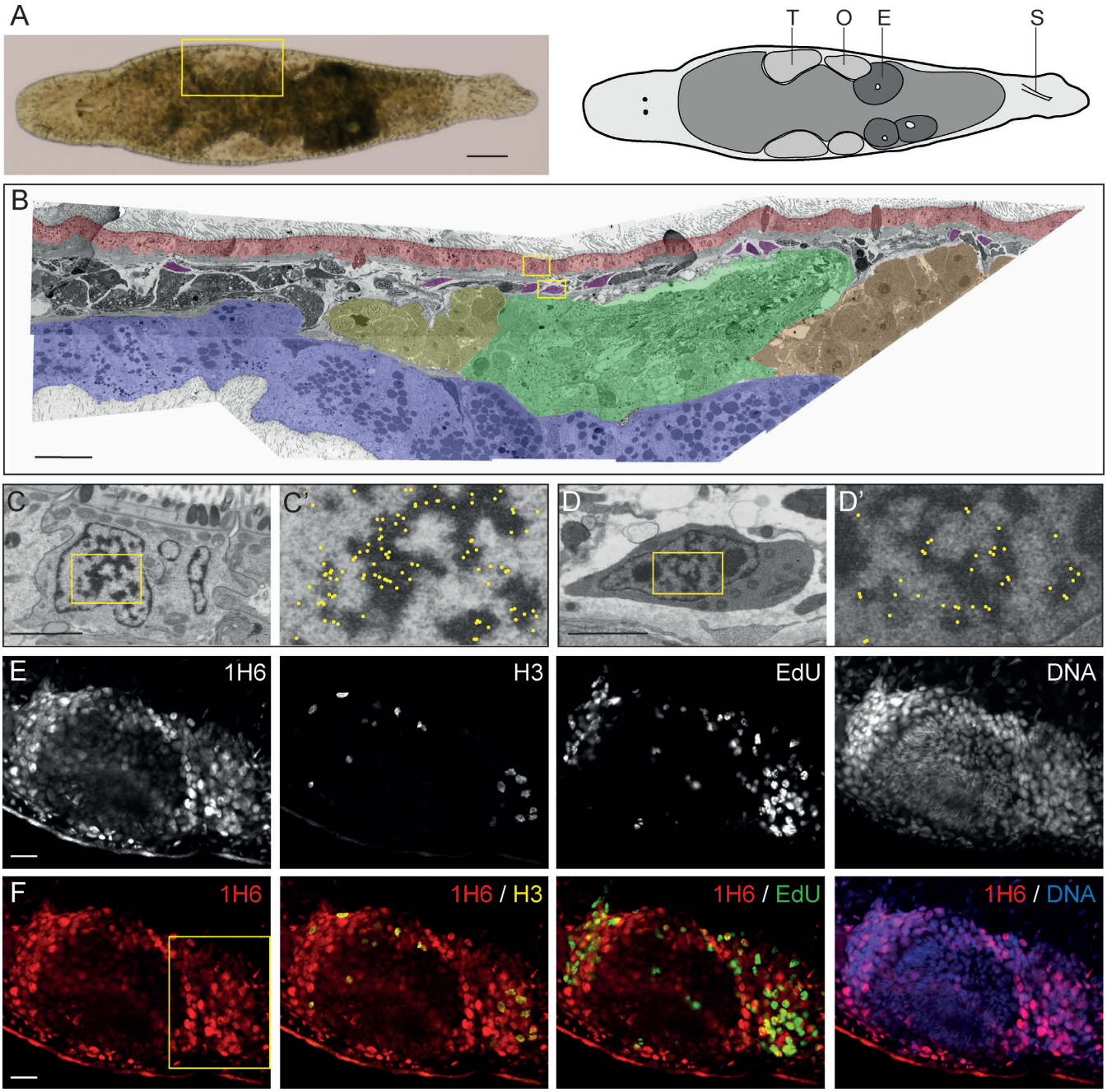

Figure 2. Weak 1H6 staining of proliferating cells in adult *Macrostomum*. (**A**) Bright-field image and schematic overview of *Macrostomum lignano*. T: Testis, O: Ovary, E: Egg and S: Stylet. (**B**) False-colored overview of 1H6 immuno-EM nanotomy data of Figure 2 available at http://www.nanotomy.org/. Red: Epidermis; Blue: Gut; Yellow: Testis Tip; Green: Testis; Orange: Ovary; Purple: somatic stem cells (neoblasts). (**C–D'**) EM images of an epidermal cell (C, C') and a neoblast (D, D') following labeling with 1H6 antibody. Boxed areas in B are shown in C and D. Boxed area in C and D are shown in C' and D'. For clarity, the immunogold particles are marked manually with yellow dots in C' and D' (raw data available online). (**E**) Gray scale images of a section through the germline. stained with 1H6, EdU (S-phase cells), phospho-H3 (mitotic cells) and DNA. (**F**) Colored overlays of sections shown in E. Higher magnifications of the boxed area in F are shown in Supplementary Figure S3. Scale bars: A: 100 μm, B: 30 μm; C, D: 2 μm; E–F: 20 μm.

co-localized in part with 1H6, in support of enrichment of G4 structures in heterochromatin (Figure 4A and B). Antibodies specific for the Suppressor of Underreplication (SUUR) protein showed an even more striking overlap with the bands labeled by 1H6 although some clear differences were also noted (Figure 4C and C', Figure 5A and A', arrows). SUUR is a SNF2 domain-containing protein that marks regions of heterochromatin and late (under-) replication (56,58,59). In contrast, bands labeled with 1H6 appeared mutually exclusive with sites of active transcription labeled by antibodies specific for RNA polymerase II (Supplementary Figure S3B). As a control we found that binding of 1H6 to polytene chromosomes could be inhibited by addition of an ≈10-fold molar excess of synthetic G4 DNA to

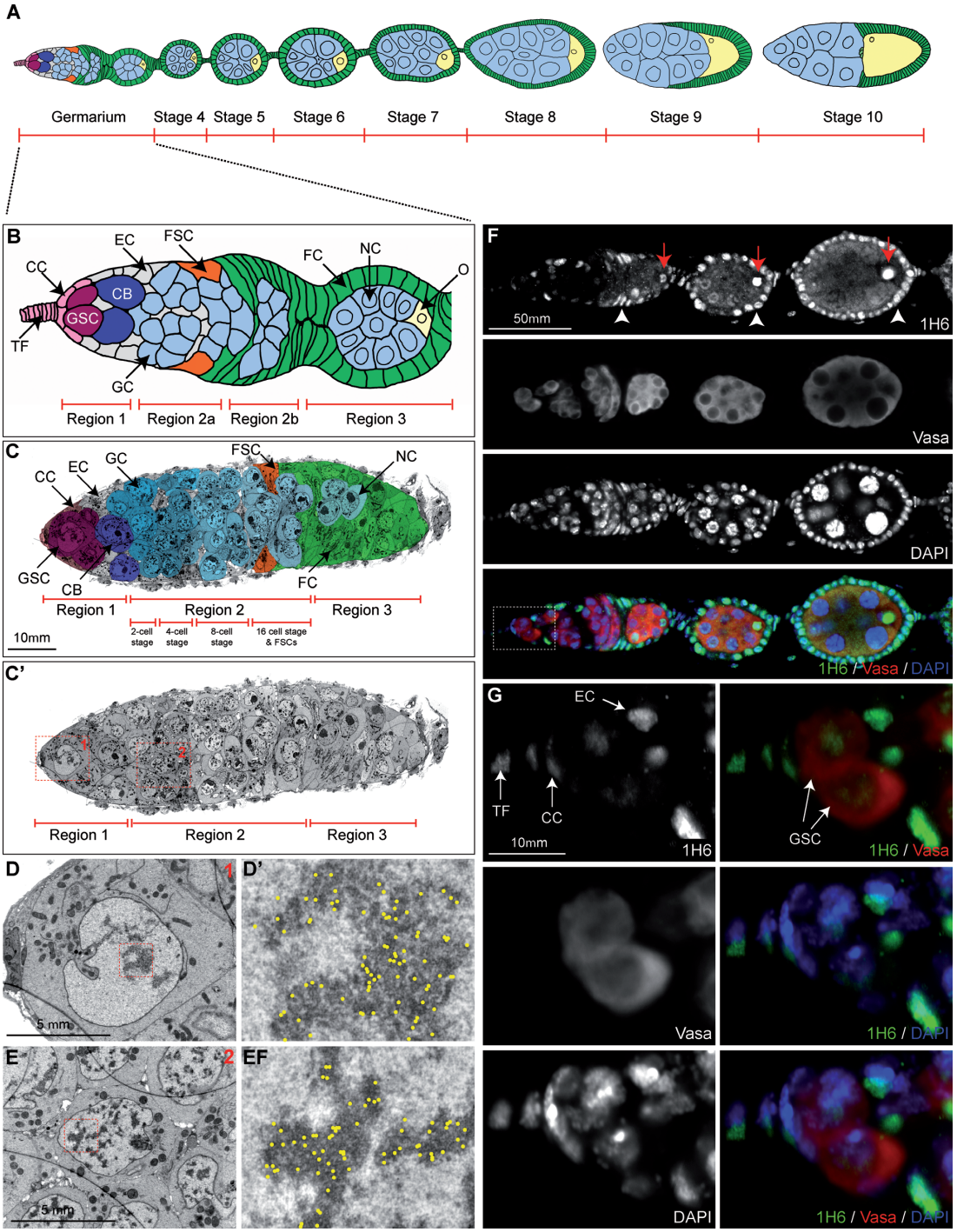

Figure 3. Germline stem cells in *Drosophila* contain less heterochromatin and stain weaker with 1H6 compared to most other cells. (**A**) Schematic diagram of a *Drosophila* ovariole up to stage 10 of egg chamber development. Green: follicle cells; light blue: nurse cells; yellow: developing oocyte. (**B**) Schematic of the germarium. TF: Terminal Filament; CC = Cap Cells; GSC: Germline Stem Cell; CB: Cystoblasts; EC: Escort Cells; GC: Germline Cysts; FSC: Follicle Stem Cells; FC: Follicle Cells; NC: Nurse Cells; O: Oocyte. (**C–E**) Overview (C,C') and close-up (D,E) images of a germarium, processed for EM and immunogold-labeled with 1H6 antibody. Nanotomy of Figure 2 shown in C' is available online at http://www.nanotomy.org). (C,C') Overview of the germarium up to stage 3. Individual cell types, identified to the best of our knowledge, were false-colored with Photoshop to match the schematic shown in B. Close-up snapshots shown in D and E correspond to the red-colored boxes in C' and depict a Germline Stem Cell (D) and Germline Cyst Cell (E) and close-ups of their heterochromatic nuclear regions respectively (D' and E'). Gold-particles, marking the presence of the 1H6-antibody, were manually marked with yellow dots (raw data available online) in D' and E'. Note the co-localization with heterochromatin. (**F** and **G**) Part of a *Drosophila* ovariole (germarium and stage 4–5, compare with schematic in A, stained with anti-1H6 (green), anti-Vasa, to indicate the germline cells (red) and the DNA dye DAPI (blue). Higher magnification images in G correspond to the white box shown in F. In the *Drosophila* germarium 1H6 antibody shows strong preference for the Terminal Filament, Cap Cells, Escort Cells (indicated in G), Follicle Cells (white arrow heads in F) and the developing oocyte (red arrows in F). This can also be seen in later stages of egg development (Supplementary Figure S2). In contrast, the Vasa-positive Germline Stem Cells, Germline Cysts and future Nurse Cells show much weaker 1H6 staining. Scale bars: C: 10 μm; D–E: 5 μm; F: 50 μm and G: 10 μm.

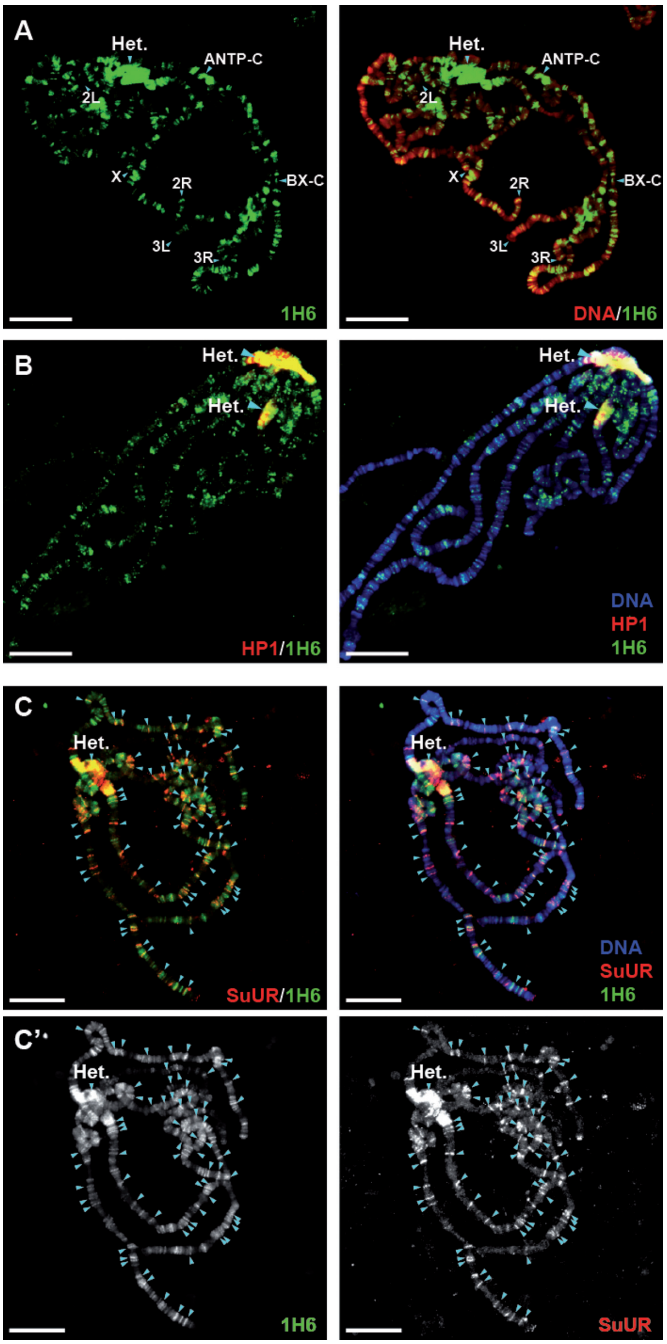

Figure 4. 1H6 staining of polytene chromosomes. (**A**) Chromosomes from salivary glands of third instar *Drosophila* larvae, stained for 1H6 (green) and the DNA dye DAPI (red). Drosophila salivary glands undergo through multiple rounds of endoreplication, resulting in polytene chromosomes that can easily be visualized with antibody staining and/or dyes. 1H6 staining reveals multiple specific loci on polytene chromosomes including pericentric heterochromatin (Het.) and developmental loci harboring *Antennapedia* (*ANTP-C*) and *Bithorax Complex* (*BX-C*). The regions of *ANTP-C* and *BX-C*, as well as pericentric heterochromatin are late replicated and underreplicated in polytene chromosomes (57). The tips of chromosome arms X, 2L, 2R, 3L and 3R are labeled. Scale bar: 25 μm. (**B**) Pericentric heterochromatin is enriched in DNA quadruplexes. Polytene chromosomes were stained with antibodies raised against Heterochromatin Protein 1 (HP1, red) and G4 DNA (1H6, green). Pericentric heterochromatin (Het.) is strongly marked with both antibodies appearing yellow when merged (right panel). Scale bar: 25 μm. (**C–C'**) G4 DNA co-localizes with the regions of late replication marked by SUUR. Polytene chromsomes were stained with SUUR (red) and 1H6 (green). The bands, which are labeled by both 1H6 and anti-SUUR antibodies are indicated by arrowheads. Note that, although most of the SUUR binding sites are also stained by 1H6, there are more additional loci stained only by 1H6. (C') Split, black and white images for 1H6 (left panel) and SUUR (right panel). Scale bar: 25 μm.

the antibody during labeling (Supplementary Figure S3A). To further study the relationship between G4 structures and SUUR we studied SUUR mutants (Figure 5B and C). In the absence of SUUR 1H6 staining was maintained (Figure 5B) but overexpression of SUUR resulted in complete loss of 1H6 staining (Figure 5C).

1H6 immuno-electron microscopy of rat pancreatic cells

To further study 1H6 binding to mammalian cells, we performed immuno-electron microscopy (EM) using the surface of ultrathin (60nm) tissue sections of rat pancreatic tissue (Figure 6). To allow the analysis of the immunogold label, used to identify 1H6, in the different cell types within this tissue, we implemented an automated large-scale electron microscopy (EM) approach known as 'nanotomy' allowing analysis of tissue cross-sections at macromolecular resolution (27,60).

Strikingly, immunogold particles localize almost exclusively to electron-dense areas of heterochromatin in the nuclei of all cells but some gold particles were also present in mitochondria and in the cytoplasmic side of the endoplasmic reticulum illustrating the resolution of our approach (Figure 6, Table 1). Previously, we showed that murine and human metaphase chromosomes were labeled by 1H6 in a non-random manner (26). Immuno-EM of a cultured pancreatic cell line confirmed 1H6 staining of mitotic chromosomes (Supplementary Figure S4a and b). Examination of nucleoli in our 1H6 nanotomy data revealed that these structures, surrounded by heterochromatin labeled by 1H6, are themselves devoid of G4 DNA staining (Supplementary Figure S5A). Note that kinetochores, identified by associated microtubules and their typical ultrastructure appearance, are also devoid of gold label (Supplementary Figure S5B).

DISCUSSION

Here we report that monoclonal antibody 1H6, specific for G4 DNA (26), has exquisite specificity for heterochromatic areas in the nucleus, condensed DNA in mitotic chromosomes and heterochromatic bands in polytene chromosomes from *Drosophila*. Striking differences in 1H6 staining were observed between cells of the soma and cells of the germline in ciliates, flatworms and flies. In these species G4 staining ranged from low to undetectable (neoblasts and germline stem cells in all species tested) to easily detectable and very strong (most somatic cells and oocytes in *Drosophila*).

Staining of G4 structures using antibodies was first described over a decade ago (32). Compared to the phage display antibodies used in that study, we observed very similar but stronger staining by the 1H6 antibody of *Stylonychia*

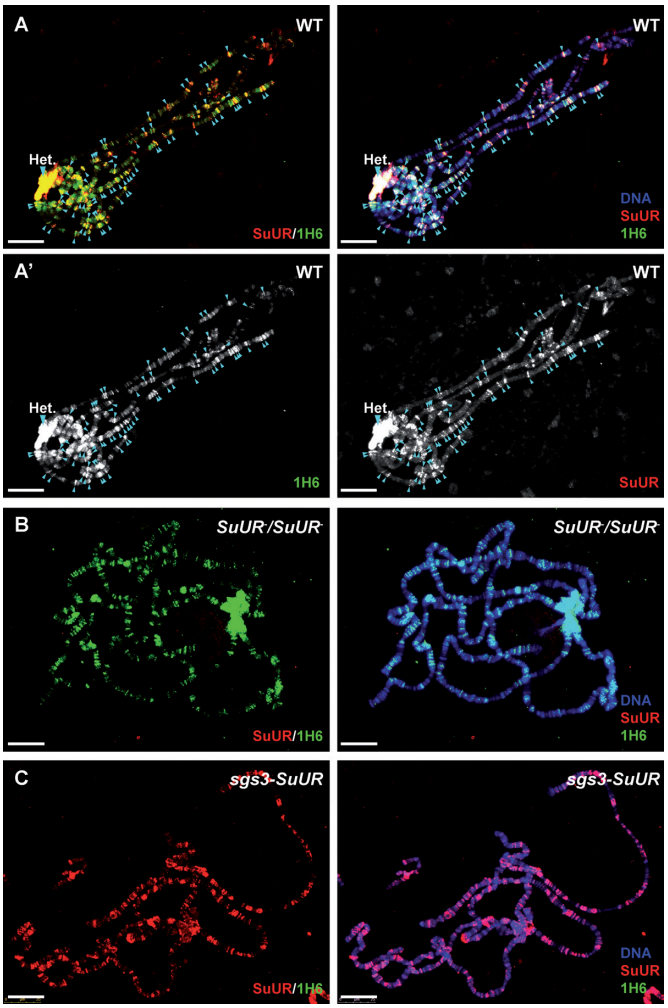

Figure 5. Loss of G4 structures upon overexpression of SUUR. (**A–A'**) In polytene chromosomes of wild type third instar *Drosophila* larvae, nearly all SUUR binding loci co-localize with G4 DNA (arrowheads) labeled by anti-SUUR (red) and 1H6 (green) antibodies. (A') Split, black and white images for 1H6 (left panel) and SUUR (right panel). (**B**) In polytene chromsomes of larvae homozygous for SUUR mutant allele G4 DNA loci are retained. Polytene chromsomes were stained with SUUR (red) and 1H6 (green). Note that SUUR staining is absent. (**C**) In polytene chromosomes of larvae overexpressing SUUR under the control of salivary gland specific GAL4 driver (sgs3), 1H6 staining is lost. Polytene chromosomes were stained with SUUR (red) and 1H6 (green). Note the increased intensity of SUUR staining. Scale bar: 25 μm.

lemnea: punctate staining of the macronucleus with the exception of the replication band and no staining of the micronucleus with germline DNA (Figure 1). Loss of G4 DNA during replication is in agreement with the earlier studies in ciliates (32), suggesting that G4 structures in the macronucleus occurs are only resolved upon DNA replication (61).

Our results support enrichment of G4 structures in heterochromatin. For our immuno-electron microscopy studies cells and tissues were cross-linked with glutaraldehyde prior to embedding in plastic, sectioning and antibody incubation. In view of this procedure the induction of G4 structures by 1H6 during antibody incubation seems very unlikely. Cross-reactivity of 1H6 with other, unknown epitopes is more difficult to exclude. For now we assume that 1H6 staining reflects the presence of G4 structures that currently remain rather poorly defined. Most likely at least two different type of G4 structures are recognized by 1H6: stable G4 structures that are present in heterochromatin and condensed metaphase chromosomes and presumably much more transient G4 structures that arise during replication and perhaps other DNA transactions such as transcription and recombination.

Whether the more stable G4 structures contribute to heterochromatin formation or are formed following heterochromatin formation is currently not known. Both principles could apply. Once formed, G4 structures could function to stabilize heterochromatin and thereby stabilize transcriptional silencing (62). This notion is supported by our observation that 1H6 bands in polytene chromosomes from *Drosophila* salivary glands are mutually exclusive with sites of transcription marked by antibodies against RNA polymerase II (Supplementary Figure S3B).

Outside the nucleus we observed sporadic 1H6 immunogold particles in the cytoplasmic site of the endoplasmatic reticulum and in mitochondria (Table 1 and Figure 6). These observations suggest that G4 structures are also present in some RNA species and in mitochondria. The availability of a monoclonal antibody that works in post-embedding immuno-EM should greatly facilitate additional studies on the role of G4 structures in various biological processes. Ideally such further studies should also report raw data in the 'nanotomy' format presented here rather than showing 'selected' images.

The partial co-localization of G4 structures with the SUUR protein is of great interest (Figure 5). Loss of SUUR is known to restore the differences in DNA copy number in polytene chromosomes (55,58). The observation that 1H6 staining persist in the absence of SUUR suggest that the formation of G4 structures does not depend on SUUR and that G4 structures themselves do not block replication. In contrast, overexpression of SUUR results in loss of 1H6 staining and increased underreplication. The binding of SUUR to polytene chromosomes was shown to be dynamic (63) and SUUR was shown to associate with the replication fork (56). Overexpression of SUUR is also known to stall replication forks and induce a DNA damage response as shown by accumulation of γH2Av co-localizing with SUUR (64). To reconcile these various findings we propose that SUUR could play a role in the resolution of G4 structures and competes with other, limiting, proteins or molecular complexes required to resolve G4 structures at the replication fork (65). A possible role for SUUR in the resolution of heterochromatin is supported by previous studies showing that over-expression of SUUR results in remarkable swellings in polytene chromosomes that are transcriptionally silent (66).

The precise nature of the epitopes recognized by 1H6 in cells and chromosomes is currently unclear. Epitopes could form on folded single strands of DNA or RNA or involve interactions between multiple molecules (Supplementary Figure S6). Unfortunately our ongoing attempts to characterize the DNA in chromatin that is enriched for 1H6 binding sites have thus far been unsuccessful (26). Whether this reflects instability of G4 structures under laboratory conditions or a failure to effectively crosslink or amplify the

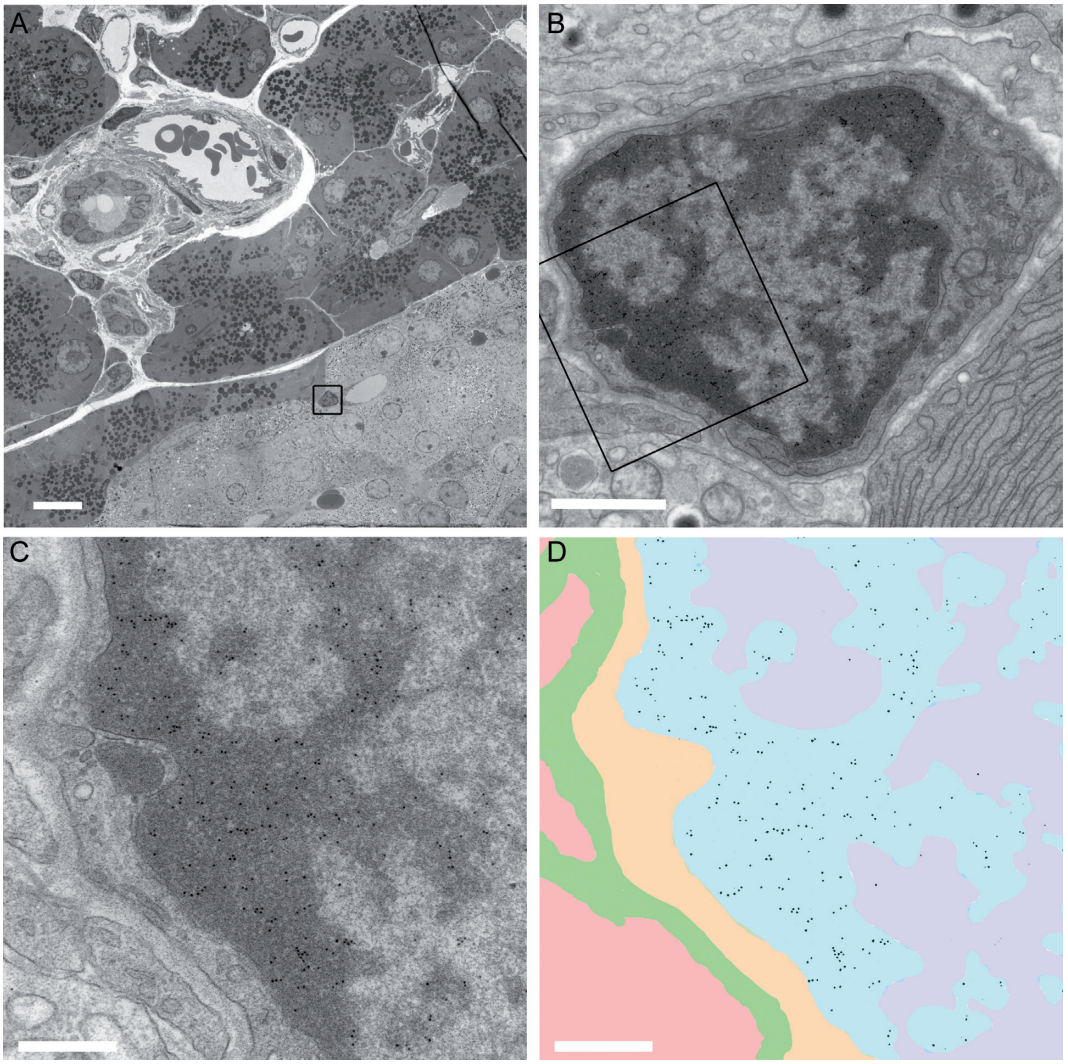

Figure 6. 1H6 binds to heterochromatin in different cells of rat pancreas. (**A**) Overview of pancreatic tissue with alpha cells, beta cells, endothelial cells, epithelial cells and exocrine cells. The different cell types can be recognized as described (www.nanotomy.nl) (27). A high-resolution 'nanotomy' digital file of Figure 6, were gold-particles can be detected in a 'Google-earth' like analysis, is available online at http://www.nanotomy.org/). The boxed area in (**A**) is shown in (**B**). The boxed area in (**B**) is shown in (**C**) and (**D**). Annotation of the ultrastructure (**C**) is illustrated in (**D**) as follows: heterochromatin blue; euchromatin purple; cytoplasm yellow; extracellular space in green and an adjacent cell (cytoplasm) in pink. The data of panel (C) were processed to selectively visualize the gold particles (black). Bars: A: 10 μm; B: 1 μm; C,D: 0.5 μm.

Table 1. Enumeration of the number and location of immunogold particles observed by immune-electron microscopy in islet of Langerhans cells of rat pancreas. Results of indirect immunogold labeling with 1H6 and an IgG2b isotype control (MOPC-141; Sigma). Raw data of this experiment is available as Figure 6 online at: http://www.nanotomy.org/). Abbreviations: Exp = experiment; Mab = monoclonal antibody used; [c] = concentration of antibody used for staining in microgram/ml; *n* = number of cells analyzed; n gold/cell = average number of gold particles per cell; Het = number of gold particles present in heterochromatin; Eu = number of gold particles present in euchromatin; H/E ratio = number of gold particles present in heterochromatin relative to the number of gold particles present in euchromatin; mito = mitochondria; ER = endoplasmatic reticulum; ER cyto = cytoplasmic side of the ER; ER lumen = luminal side of the ER; ER C/L ratio = ratio of the number of gold particles present in the cytoplasmic versus the luminal side of the ER; ctr = isotype control antibody

Exp	Mab	[c]	Cells (n)	n gold/cell	Nucleus				Cytoplasm					
					total	Het	Eu	H/E ratio	total	mito	ER	ER cyto	ER lumen	ER C/L ratio
1	1H6	1	77	155.1	140.6	125.0	15.6	0.88	14.5	1.1	1.3	17.9	1.9	0.92
	ctr	1	83	2.5	1.3	1.2	0.2	0.68	1.2	0.2	n.d.	n.d	n.d	n.d.
2	1H6	1	30	943.5	718.8	672.5	46.2	0.93	224.5	11.2	66.4	62.6	3.8	0.94
	ctr	1	30	7.0	1.9	1.5	0.4	0.79	5.1	0.9	3.5	3	0.5	0.85
	1H6	0.2	25	319.6	236.6	253.0	17.0	0.93	83.0	5.8	40.3	37.4	2.9	0.92
	ctr	0.2	30	13.7	3.5	2.5	1.0	0.74	10.2	0.6	5.1	4.1	1	0.80

DNA in these structures in a way that is compatible with fragmentation and construction of sequencing libraries is currently not known. However, we previously showed that 1H6 reacts with intra- as well as intermolecular G4 DNA structures (26) and both types of G4 structures could be present *in vivo* (Supplementary Figure S6). The G4 structures recognized by 1H6 could also contain RNA and/or DNA (67–69). Whereas the affinity of 1H6 for G4 DNA is higher than for G4 RNA ((26) and unpublished observations), the distinction between *in situ* binding of 1H6 to G4 RNA, G4 DNA or hybrid G4 DNA/RNA structures is not trivial since the activity of various RNAases on (fixed) G4 structures containing RNA remains to be established. Epitopes recognized by 1H6 could also be present in G4 structures composed of two or four partially double stranded DNA molecules (Supplementary Figure S6).

Previous studies have shown that DNA capable of G4 DNA is not randomly distributed throughout the genome (70). In plants, G4 motifs are enriched at genes coupled to energy status and signaling pathways (71). It has been estimated that there are more than 300 000 sites with this potential in the human genome (14–16). If the potential to form G4 structures is not limited to four runs of guanine repeats and includes hybrid DNA/RNA structures with one or more G-rich transcripts (Supplementary Figure S6), G4 structures could form at many more locations including, for example, at telomeres in yeast and at telomeric transposons in *Drosophila melanogaster* (72). Another possibility is that molecular crowding, shown to dissociate duplex telomeric DNA into G4 DNA (23), could induce the formation of intermolecular G4 DNA structures in cells in the absence of specific RNA transcripts. The molecular characterization of the G4 structures recognized by 1H6 as well as the further mapping of 1H6 binding sites in different cells and chromosomes are important objectives for future studies.

Our results indicate that G4 structures are present in postmitotic cells as well as in mitotic chromosomes. These observations suggest that G4 structures can exist independent of DNA replication, transcription or recombination. In general, the presence of G4 structures in cells could provide a challenge to genome stability. Given the variable presence of G4 structures in different cells such genomic instability could be cell type specific (compare, e.g. GSC and oocytes in Figure 3). Instability of G-rich DNA could occur when G4 structures need to be resolved prior to transcription, replication, repair or homologous recombination. Failure to unwind G4 structures could result in contraction and expansions of G-rich repeats. Expansions of G-rich repeats could increase the probability of G4 formation and favor sequestration of genomic regions around such repeat expansions into silent heterochromatin. This mechanism provides an attractive explanation for the reported link between the length of G-rich repeats and the suppression of globin gene expression in patients with ATR-X syndrome (73) and the length of $(GGGGCC)_n$ and $(CGG)_n$ repeats and suppression of gene expression in neurodegenerative diseases (74,75). It is tempting to speculate that differences in the stability of G-rich repeats between somatic cells and cells of the germline are related to differences in the way G4 structures are formed or are processed in these different cell types. Future studies will examine this intriguing possibility and clarify the emerging role of G4 structures in nuclear organization, gene expression, telomere function and cell differentiation.

SUPPLEMENTARY DATA

Supplementary Data are available at NAR Online.

ACKNOWLEDGEMENTS

We thank Piet Borst, Tom Cech, Rudolf Jaenisch, Christopher Pearson and Bas van Steensel for comments on the manuscript, Ester Falconer, Alexander Henderson, Evert-Jan Uringa, Sarra Merzouk and Diana Spierings for discussions and Nancy Halsema, Inge Kazemier and Sandra Henkelman for help with experiments.
Author Contributions: R.H., Y.M.M., S.M., N.A.G., R.D.K., A.V.R., J.K., A.H.G.W., K.N., A.V.R. J.P. performed experiments, analyzed data and prepared figures. Y.M.M., S.M., E.B., J.P., H.L., O.C.M.S. and B.N.G.G helped with the design of the experiments, performed data analysis and edited the manuscript. P.M.L designed the research, analyzed data and wrote the manuscript.

FUNDING

Netherlands Organization for Scientific Research [NWO175-010-2009-023, ZonMW91111006; STW12718; ALW 86510012]; Canadian Institute of Health Research [MOP38075]; National Institute of Health [GMH79042]; Russian Science Foundation [14-14-00221 to A.V.R.]. P.M.L. is a recipient of an Advanced ERC grant. Funding for open access charge: University Medical Center Groningen, the Netherlands.
Conflict of interest statement. None declared.

REFERENCES

1. Jost,K.L., Bertulat,B. and Cardoso,M.C. (2012) Heterochromatin and gene positioning: inside, outside, any side? *Chromosoma*, **121**, 555–563.
2. Passarge,E. (1979) Emil Heitz and the concept of heterochromatin: longitudinal chromosome differentiation was recognized fifty years ago. *Am. J. Hum. Genet.*, **31**, 106–115.
3. Woodcock,C.L. and Ghosh,R.P. (2010) Chromatin higher-order structure and dynamics. *Cold Spring Harb. Perspect. Biol.*, **2**, a000596.
4. Bickmore,W.A. and van Steensel,B. (2013) Genome architecture: domain organization of interphase chromosomes. *Cell*, **152**, 1270–1284.
5. Hubner,M.R., Eckersley-Maslin,M.A. and Spector,D.L. (2013) Chromatin organization and transcriptional regulation. *Curr. Opin. Genet. Dev.*, **23**, 89–95.
6. Fussner,E., Ching,R.W. and Bazett-Jones,D.P. (2011) Living without 30nm chromatin fibers. *Trends Biochem. Sci.*, **36**, 1–6.
7. Nishino,Y., Eltsov,M., Joti,Y., Ito,K., Takata,H., Takahashi,Y., Hihara,S., Frangakis,A.S., Imamoto,N., Ishikawa,T. *et al.* (2012) Human mitotic chromosomes consist predominantly of irregularly folded nucleosome fibres without a 30-nm chromatin structure. *EMBO J.*, **31**, 1644–1653.
8. Hansen,J.C. (2012) Human mitotic chromosome structure: what happened to the 30-nm fibre? *EMBO J.*, **31**, 1621–1623.
9. Sen,D. and Gilbert,W. (1992) Guanine quartet structures. *Methods Enzymol.*, **211**, 191–199.
10. Lane,A.N. (2012) The stability of intramolecular DNA G-quadruplexes compared with other macromolecules. *Biochimie*, **94**, 277–286.

11. Bucek,P., Jaumot,J., Avino,A., Eritja,R. and Gargallo,R. (2009) pH-Modulated Watson-Crick duplex-quadruplex equilibria of guanine-rich and cytosine-rich DNA sequences 140 base pairs upstream of the c-kit transcription initiation site. *Chemistry*, **15**, 12663–12671.
12. Rodriguez Lopez,C.M., Guzman Asenjo,B., Lloyd,A.J. and Wilkinson,M.J. (2010) Direct detection and quantification of methylation in nucleic acid sequences using high-resolution melting analysis. *Anal. Chem.*, **82**, 9100–9108.
13. Li,D., Lv,B., Zhang,H., Lee,J.Y. and Li,T. (2014) Positive supercoiling affiliated with nucleosome formation repairs non-B DNA structures. *Chem. Commun. (Camb.)*, **50**, 10641–10644.
14. Tran,P.L., Mergny,J.L. and Alberti,P. (2011) Stability of telomeric G-quadruplexes. *Nucleic acids Res.*, **39**, 3282–3294.
15. Huppert,J.L. and Balasubramanian,S. (2005) Prevalence of quadruplexes in the human genome. *Nucleic Acids Res.*, **33**, 2908–2916.
16. Todd,A.K., Johnston,M. and Neidle,S. (2005) Highly prevalent putative quadruplex sequence motifs in human DNA. *Nucleic Acids Res.*, **33**, 2901–2907.
17. Maizels,N. and Gray,L.T. (2013) The G4 genome. *PLoS Genet.*, **9**, e1003468.
18. Duquette,M.L., Handa,P., Vincent,J.A., Taylor,A.F. and Maizels,N. (2004) Intracellular transcription of G-rich DNAs induces formation of G-loops, novel structures containing G4 DNA. *Genes Dev.*, **18**, 1618–1629.
19. Cheung,I., Schertzer,M., Rose,A. and Lansdorp,P.M. (2002) Disruption of dog-1 in Caenorhabditis elegans triggers deletions upstream of guanine-rich DNA. *Nat. Genet.*, **31**, 405–409.
20. Kruisselbrink,E., Guryev,V., Brouwer,K., Pontier,D.B., Cuppen,E. and Tijsterman,M. (2008) Mutagenic capacity of endogenous G4 DNA underlies genome instability in FANCJ-defective C. elegans. *Curr. Biol.*, **18**, 900–905.
21. Ribeyre,C., Lopes,J., Boule,J.B., Piazza,A., Guedin,A., Zakian,V.A., Mergny,J.L. and Nicolas,A. (2009) The yeast Pif1 helicase prevents genomic instability caused by G-quadruplex-forming CEB1 sequences in vivo. *PLoS Genet.*, **5**, e1000475.
22. Bonetti,D., Martina,M., Falcettoni,M. and Longhese,M.P. (2013) Telomere-end processing: mechanisms and regulation. *Chromosoma*, **123**, 57–66.
23. Miyoshi,D., Matsumura,S., Nakano,S. and Sugimoto,N. (2004) Duplex dissociation of telomere DNAs induced by molecular crowding. *J. Am. Chem. Soc.*, **126**, 165–169.
24. Bochman,M.L., Paeschke,K. and Zakian,V.A. (2012) DNA secondary structures: stability and function of G-quadruplex structures. *Nat. Rev. Genet.*, **13**, 770–780.
25. Wolfe,A.L., Singh,K., Zhong,Y., Drewe,P., Rajasekhar,V.K., Sanghvi,V.R., Mavrakis,K.J., Jiang,M., Roderick,J.E., Van der Meulen,J. *et al.* (2014) RNA G-quadruplexes cause eIF4A-dependent oncogene translation in cancer. *Nature*, **513**, 65–70.
26. Henderson,A., Wu,Y., Huang,Y.C., Chavez,E.A., Platt,J., Johnson,F.B., Brosh,R.M. Jr, Sen,D. and Lansdorp,P.M. (2014) Detection of G-quadruplex DNA in mammalian cells. *Nucleic Acids Res.*, **42**, 860–869.
27. Ravelli,R.B., Kalicharan,R.D., Avramut,M.C., Sjollema,K.A., Pronk,J.W., Dijk,F., Koster,A.J., Visser,J.T., Faas,F.G. and Giepmans,B.N. (2013) Destruction of tissue, cells and organelles in type 1 diabetic rats presented at macromolecular resolution. *Sci. Rep.*, **3**, 1804.
28. Postberg,J., Heyse,K., Cremer,M., Cremer,T. and Lipps,H.J. (2008) Spatial and temporal plasticity of chromatin during programmed DNA-reorganization in Stylonychia macronuclear development. *Epigenetics Chromatin*, **1**, 3.
29. McCloy,R.A., Rogers,S., Caldon,C.E., Lorca,T., Castro,A. and Burgess,A. (2014) Partial inhibition of Cdk1 in G 2 phase overrides the SAC and decouples mitotic events. *Cell Cycle*, **13**, 1400–1412.
30. Klobutcher,L.A., Swanton,M.T., Donini,P. and Prescott,D.M. (1981) All gene-sized DNA molecules in four species of hypotrichs have the same terminal sequence and an unusual 3' terminus. *Proc. Natl. Acad. Sci. U.S.A.*, **78**, 3015–3019.
31. Aeschlimann,S.H., Jonsson,F., Postberg,J., Stover,N.A., Petera,R.L., Lipps,H.J., Nowacki,M. and Swart,E.C. (2014) The draft assembly of the radically organized Stylonychia lemnae macronuclear genome. *Genome Biol. Evol.*, **6**, 1707–1723.
32. Schaffitzel,C., Berger,I., Postberg,J., Hanes,J., Lipps,H.J. and Pluckthun,A. (2001) In vitro generated antibodies specific for telomeric guanine-quadruplex DNA react with Stylonychia lemnae macronuclei. *Proc. Natl. Acad. Sci. U.S.A.*, **98**, 8572–8577.
33. Paeschke,K., Simonsson,T., Postberg,J., Rhodes,D. and Lipps,H.J. (2005) Telomere end-binding proteins control the formation of G-quadruplex DNA structures in vivo. *Nat. Struct. Mol. Biol.*, **12**, 847–854.
34. Jonsson,F., Postberg,J., Schaffitzel,C. and Lipps,H.J. (2002) Organization of the macronuclear gene-sized pieces of stichotrichous ciliates into a higher order structure via telomere-matrix interactions. *Chromosome Res.*, **10**, 445–453.
35. Lipps,H.J. (1980) In vitro aggregation of the gene-sized DNA molecules of the ciliate Stylonychia mytilus. *Proc. Natl. Acad. Sci. U.S.A.*, **77**, 4104–4107.
36. Lipps,H.J., Gruissem,W. and Prescott,D.M. (1982) Higher order DNA structure in macronuclear chromatin of the hypotrichous ciliate Oxytricha nova. *Proc. Natl. Acad. Sci. U.S.A.*, **79**, 2495–2499.
37. Sundquist,W.I. and Klug,A. (1989) Telomeric DNA dimerizes by formation of guanine tetrads between hairpin loops. *Nature*, **342**, 825–829.
38. Murti,K.G. and Prescott,D.M. (1983) Replication forms of the gene-sized DNA molecules of hypotrichous ciliates. *Mol. Cell. Biol.*, **3**, 1562–1566.
39. Postberg,J., Alexandrova,O., Cremer,T. and Lipps,H.J. (2005) Exploiting nuclear duality of ciliates to analyse topological requirements for DNA replication and transcription. *J. Cell Sci.*, **118**, 3973–3983.
40. Gottschling,D.E. and Zakian,V.A. (1986) Telomere proteins: specific recognition and protection of the natural termini of Oxytricha macronuclear DNA. *Cell*, **47**, 195–205.
41. Paeschke,K., Juranek,S., Rhodes,D. and Lipps,H.J. (2008) Cell cycle-dependent regulation of telomere tethering in the nucleus. *Chromosome Res.*, **16**, 721–728.
42. Paeschke,K., Juranek,S., Simonsson,T., Hempel,A., Rhodes,D. and Lipps,H.J. (2008) Telomerase recruitment by the telomere end binding protein-beta facilitates G-quadruplex DNA unfolding in ciliates. *Nat. Struct. Mol. Biol.*, **15**, 598–604.
43. Ding,H., Schertzer,M., Wu,X., Gertsenstein,M., Selig,S., Kammori,M., Pourvali,R., Poon,S., Vulto,I., Chavez,E. *et al.* (2004) Regulation of murine telomere length by Rtel: an essential gene encoding a helicase-like protein. *Cell*, **117**, 873–886.
44. Vannier,J.B., Pavicic-Kaltenbrunner,V., Petalcorin,M.I., Ding,H. and Boulton,S.J. (2012) RTEL1 dismantles T loops and counteracts telomeric G4-DNA to maintain telomere integrity. *Cell*, **149**, 795–806.
45. Wagner,D.E., Ho,J.J. and Reddien,P.W. (2012) Genetic regulators of a pluripotent adult stem cell system in planarians identified by RNAi and clonal analysis. *Cell Stem Cell*, **10**, 299–311.
46. Ladurner,P., Scharer,L., Salvenmoser,W. and Rieger,R.M. (2005) A new model organism among the lower Bilateria and the use of digital microscopy in taxonomy of meiobenthic Platyhelminthes: Macrostomum lignano, n. sp (Rhabditophora, Macrostomorpha). *J. Zool. Syst. Evol. Res.*, **43**, 114–126.
47. Xi,R. and Xie,T. (2005) Stem cell self-renewal controlled by chromatin remodeling factors. *Science*, **310**, 1487–1489.
48. Ladurner,P., Rieger,R. and Baguna,J. (2000) Spatial distribution and differentiation potential of stem cells in hatchlings and adults in the marine platyhelminth macrostomum sp.: a bromodeoxyuridine analysis. *Dev. Biol.*, **226**, 231–241.
49. Lin,H. (2002) The stem-cell niche theory: lessons from flies. *Nat. Rev. Genet.*, **3**, 931–940.
50. Spradling,A., Drummond-Barbosa,D. and Kai,T. (2001) Stem cells find their niche. *Nature*, **414**, 98–104.
51. Rieger,R.M., Legniti,A., Ladurner,P., Reiter,D., Asch,E., Salvenmoser,W., Schurmann,W. and Peter,R. (1999) Ultrastructure of neoblasts in microturbellaria: significance for understanding stem cells in free-living Platyhelminthes. *Invert. Reprod. Dev.*, **35**, 127–140.
52. Mouton,S., Willems,M., Braeckman,B.P., Egger,B., Ladurner,P., Scharer,L. and Borgonie,G. (2009) The free-living flatworm Macrostomum lignano: a new model organism for ageing research. *Exp. Gerontol.*, **44**, 243–249.

53. van Wolfswinkel,J.C., Wagner,D.E. and Reddien,P.W. (2014) Single-cell analysis reveals functionally distinct classes within the planarian stem cell compartment. *Cell Stem Cell*, **15**, 326–339.
54. Rudkin,G.T. (1969) Non replicating DNA in Drosophila. *Genetics*, **61** (Suppl), 227–238.
55. Nordman,J., Li,S., Eng,T., Macalpine,D. and Orr-Weaver,T.L. (2011) Developmental control of the DNA replication and transcription programs. *Genome Res.*, **21**, 175–181.
56. Nordman,J.T., Kozhevnikova,E.N., Verrijzer,C.P., Pindyurin,A.V., Andreyeva,E.N., Shloma,V.V., Zhimulev,I.F. and Orr-Weaver,T.L. (2014) DNA copy-number control through inhibition of replication fork progression. *Cell Rep.*, **9**, 841–849.
57. Moshkin,Y.M., Alekseyenko,A.A., Semeshin,V.F., Spierer,A., Spierer,P., Makarevich,G.F., Belyaeva,E.S. and Zhimulev,I.F. (2001) The bithorax complex of Drosophila melanogaster: Underreplication and morphology in polytene chromosomes. *Proc. Natl. Acad. Sci. U.S.A.*, **98**, 570–574.
58. Belyaeva,E.S., Zhimulev,I.F., Volkova,E.I., Alekseyenko,A.A., Moshkin,Y.M. and Koryakov,D.E. (1998) Su(UR)ES: a gene suppressing DNA underreplication in intercalary and pericentric heterochromatin of Drosophila melanogaster polytene chromosomes. *Proc. Natl. Acad. Sci. U.S.A.*, **95**, 7532–7537.
59. Pindyurin,A.V., Boldyreva,L.V., Shloma,V.V., Kolesnikova,T.D., Pokholkova,G.V., Andreyeva,E.N., Kozhevnikova,E.N., Ivanoschuk,I.G., Zarutskaya,E.A., Demakov,S.A. *et al.* (2008) Interaction between the Drosophila heterochromatin proteins SUUR and HP1. *J. Cell Sci.*, **121**, 1693–1703.
60. Faas,F.G., Avramut,M.C., van den Berg,B.M., Mommaas,A.M., Koster,A.J. and Ravelli,R.B. (2012) Virtual nanoscopy: generation of ultra-large high resolution electron microscopy maps. *J. Cell Biol.*, **198**, 457–469.
61. Postberg,J., Tsytlonok,M., Sparvoli,D., Rhodes,D. and Lipps,H.J. (2012) A telomerase-associated RecQ protein-like helicase resolves telomeric G-quadruplex structures during replication. *Gene*, **497**, 147–154.
62. Gray,L.T., Vallur,A.C., Eddy,J. and Maizels,N. (2014) G quadruplexes are genomewide targets of transcriptional helicases XPB and XPD. *Nat. Chem. Biol.*, **10**, 313–318.
63. Kolesnikova,T.D., Posukh,O.V., Andreyeva,E.N., Bebyakina,D.S., Ivankin,A.V. and Zhimulev,I.F. (2013) Drosophila SUUR protein associates with PCNA and binds chromatin in a cell cycle-dependent manner. *Chromosoma*, **122**, 55–66.
64. Andreyeva,E.N., Kolesnikova,T.D., Belyaeva,E.S., Glaser,R.L. and Zhimulev,I.F. (2008) Local DNA underreplication correlates with accumulation of phosphorylated H2Av in the Drosophila melanogaster polytene chromosomes. *Chromosome Res.*, **16**, 851–862.
65. Lopes,J., Piazza,A., Bermejo,R., Kriegsman,B., Colosio,A., Teulade-Fichou,M.P., Foiani,M. and Nicolas,A. (2011) G-quadruplex-induced instability during leading-strand replication. *EMBO J.*, **30**, 4033–4046.
66. Zhimulev,I.F., Belyaeva,E.S., Semeshin,V.F., Shloma,V.V., Makunin,I.V. and Volkova,E.I. (2003) Overexpression of the SuUR gene induces reversible modifications at pericentric, telomeric and intercalary heterochromatin of Drosophila melanogaster polytene chromosomes. *J. Cell Sci*, **116**, 169–176.
67. Xu,Y., Kimura,T. and Komiyama,M. (2008) Human telomere RNA and DNA form an intermolecular G-quadruplex. *Nucleic Acids Symp. Ser.*, **52**, 169–170.
68. Wanrooij,P.H., Uhler,J.P., Shi,Y., Westerlund,F., Falkenberg,M. and Gustafsson,C.M. (2012) A hybrid G-quadruplex structure formed between RNA and DNA explains the extraordinary stability of the mitochondrial R-loop. *Nucleic Acids Res.*, **40**, 10334–10344.
69. Cao,K., Ryvkin,P. and Johnson,F.B. (2012) Computational detection and analysis of sequences with duplex-derived interstrand G-quadruplex forming potential. *Methods*, **57**, 3–10.
70. Eddy,J. and Maizels,N. (2008) Conserved elements with potential to form polymorphic G-quadruplex structures in the first intron of human genes. *Nucleic Acids Res.*, **36**, 1321–1333.
71. Andorf,C.M., Kopylov,M., Dobbs,D., Koch,K.E., Stroupe,M.E., Lawrence,C.J. and Bass,H.W. (2014) G-quadruplex (G4) motifs in the maize (Zea mays L.) genome are enriched at specific locations in thousands of genes coupled to energy status, hypoxia, low sugar, and nutrient deprivation. *Yi Chuan Xue Bao*, **41**, 627–647.
72. Abad,J.P. and Villasante,A. (1999) The 3' non-coding region of the Drosophila melanogaster HeT-A telomeric retrotransposon contains sequences with propensity to form G-quadruplex DNA. *FEBS Lett.*, **453**, 59–62.
73. Law,M.J., Lower,K.M., Voon,H.P., Hughes,J.R., Garrick,D., Viprakasit,V., Mitson,M., De Gobbi,M., Marra,M., Morris,A. *et al.* (2010) ATR-X syndrome protein targets tandem repeats and influences allele-specific expression in a size-dependent manner. *Cell*, **143**, 367–378.
74. Haeusler,A.R., Donnelly,C.J., Periz,G., Simko,E.A., Shaw,P.G., Kim,M.S., Maragakis,N.J., Troncoso,J.C., Pandey,A., Sattler,R. *et al.* (2014) C9orf72 nucleotide repeat structures initiate molecular cascades of disease. *Nature*, **507**, 195–200.
75. Colak,D., Zaninovic,N., Cohen,M.S., Rosenwaks,Z., Yang,W.Y., Gerhardt,J., Disney,M.D. and Jaffrey,S.R. (2014) Promoter-bound trinucleotide repeat mRNA drives epigenetic silencing in fragile X syndrome. *Science*, **343**, 1002–1005.